JOURNAL OF SOLID STATE CHEMISTRY 37, 256–263 (1981)

Synthesis and Structure of an Infinite-Chain Form of ZrI_2 (α)*

DENNIS H. GUTHRIE AND JOHN D. CORBETT

Ames Laboratory† and Department of Chemistry, Iowa State University, Ames, Iowa 50011

Received August 1, 1980; in final form October 2, 1980

The synthesis of a second polymorph of ZrI_2 has been achieved by a transport reaction between ZrI_4 and zirconium metal under a 750/850°C gradient in a sealed tantalum tube. The black lath-like crystals produced in the 775°C region occur in space group $P2_1/m$ with $a = 6.821(2)$ Å, $b = 3.741(1)$ Å, $c = 14.937(3)$ Å, $\beta = 95.66(3)°$, $Z = 4$. A total of 669 independent reflections with $2\theta \leq 50°$ and $I > 3\sigma(I)$ were measured at room temperature on a four-circle automated diffractometer with monochromatized Mo$K\alpha$ radiation and were corrected for absorption ($\mu = 190$ cm^{-1}). The structure was solved by direct methods and full-matrix least-squares refinement of all atoms with anisotropic thermal parameters to give final residuals $R = 0.064$ and $R_w = 0.079$. This phase is isoelectronic and isostructural with β-$MoTe_2$, a distorted CdI_2-type structure in which the zirconium atoms are displaced 0.440 Å from the octahedral centers along a to form infinite zigzag metal chains ($d_{Zr-Zr} = 3.182(3)$ Å) parallel to b. The phase is a diamagnetic semiconductor at room temperature ($E_g \sim 0.1$ eV).

Introduction

Several reduced zirconium halides with zirconium in an oxidation state less than 3 have recently been synthesized and characterized. Among the chlorides and bromides are the clusters Zr_6Cl_{15} (*1*) and Zr_6X_{12} (*2*), $ZrCl_2$ (3*R*-MoS_2 type) (*3*, *4*), and the double-metal-layered ZrCl (*5–7*) and ZrBr (*8*) compounds. Yet, until recently the only well-characterized zirconium iodides were ZrI_4 and ZrI_3, both known for their importance in the purification of zirconium via the van Arkel process. The triiodide has been found to be nonstoichiometric over the range $ZrI_{2.83}$ (775°C) to $ZrI_{3.43}$ (475°C), with a recognizable superstructure to X rays at the upper limit (*9*). The synthesis of a zirconium diiodide has been reported by Sale and Shelton (*10*) from the disproportionation of ZrI_3 under a 360/390°C gradient in a sealed Pyrex tube. However, the reported powder pattern has been found to correspond closely to that of the lower-limit triiodide $ZrI_{2.8}$ (*9*). Lack of earlier evidence for zirconium iodides more reduced than the ZrI_3 phase appears to have originated mainly from the use of reaction times which were too short, temperatures which were too low and, probably, glass containers. Increases in these two parameters and the use of sealed tantalum containers have enabled the synthesis of the cluster Zr_6I_{12} (*1*), and the present article reports on a second polymorph of ZrI_2, an infinite-metal-chain

† Operated for the U.S. Department of Energy by Iowa State University under Contract W-7405-Eng-82. This research was supported by the Assistant Secretary for Energy Research, Office of Basic Energy Sciences, WPAS-KC-02-02-03.

0022-4596/81/050256-08$02.00/0

form. The new phase is stable at lower temperatures (775°C) than Zr_6I_{12} (875°C) and therefore is referred to as α-ZrI_2.

Experimental Section

Materials

Reactor-grade crystal bar zirconium (<500 ppm Hf) was melted into a loaf under vacuum, cut into ~2-mm-thick slices, and these were cold rolled to strips 0.4–0.5-mm thick. The strips were then either electropolished or cleaned in acetone and then in a solution of 45% concentrated HNO_3, 45% H_2O, 10% HF to remove any hydrocarbons and surface impurities picked up during cold rolling. The strips were then washed with acetone, dried, and stored under vacuum.

The tetraiodide was prepared by reaction of gaseous, reagent-grade iodine (<0.005% Cl and Br) from a reservoir at ~150°C with excess metal heated to 350–400°C within a sealed Pyrex container. The product was purified by vacuum sublimation ($<10^{-5}$ Torr) through a coarse-grade Pyrex frit at 400°C. Transfer and manipulation of all materials was done by standard vacuum-line or drybox techniques.

Synthesis

The use of sealed tantalum tubing as a reaction vessel for high-temperature reactions involving lower halides of zirconium has proven very successful (*4, 5, 7–9*), and this approach was continued. The containers were induction cleaned (1800°C), arc welded under helium after filling, jacketed in fused silica tubes, and sealed off under vacuum. Temperatures were monitored during the reaction with thermocouples fastened to the outside of the silica jacket. Any temperature difference between the Ta container and the outside of this jacket is considered small at the temperatures involved and fairly constant from reaction to reaction.

The initial synthesis used ~1 g of ZrI_4 with a large excess of zirconium strips which extended the length of a 10 to 12-cm long, 0.95 cm o.d. tantalum tube. The reaction was carried out for 4 weeks under a 750/850°C temperature gradient after which the container was allowed to cool in the furnace. Long reaction times are required to overcome kinetic problems known in this and similar systems (*4, 11*), and the temperature gradient allowed formation of phases which might be stable only in a limited temperature region. A 10–20% yield of lath-like crystals with a high metal-like luster was found growing in the 775°C region on the zirconium strip as well as the inside walls of the tantalum tube. These are thought to have been produced via the transport reactions

$$3ZrI_4(g) + Zr(s) \overset{850°C}{\rightleftarrows} 4ZrI_3(g) \text{ (endothermic)},$$

followed by

$$2ZrI_3(g) \overset{775°C}{\rightleftarrows} \alpha\text{-}ZrI_2(s) + ZrI_4(g).$$

Subsequent reactions have indicated that the metal in the 775°C region first becomes coated with a powder and small crystals of α-ZrI_2, presumably because of the presence of a large number of nucleation sites and a high P_{ZrI_4} in the early stages of the reaction. As the reaction proceeds larger crystals are formed, sometimes up to 2 cm long. A temperature zone <775°C (750°C) is necessary to allow separation of any ZrI_3 formed from α-ZrI_2.

Data Collection

The Ta tube was opened in a drybox especially designed for crystal mounting, and suitable specimens were selected under low magnification. These were mounted within 0.2-mm (i.d.) glass capillaries which were sealed in the drybox with the aid of a hot nichrome wire and later resealed outside the box with a gas flame. The single

crystal selected for data collection was chosen with the aid of oscillation photographs and had extreme dimensions of 1.17 × 0.08 × 0.01 mm. Data for the indicated monoclinic unit cell were collected at ambient temperature on an automated four-circle diffractometer designed and built in the Ames Laboratory (*12*) using Mo$K\alpha$ radiation monochromated with a graphite crystal (λ = 0.70954 Å). All data within a sphere defined by $2\theta \leq 50°$ were collected in the HKL, HK$\bar{L}$, and H$\bar{K}\bar{L}$ octants using an ω-scan mode. Peak heights of three standard reflections did not show any significant change over the period of data collection. A total of 1427 of the 1750 reflections checked were classified as observed by the criterion $I > 3\sigma(I)$. The observed intensities were corrected for Lorentz and polarization effects after which appropriate averaging of duplicate reflections yielded 669 independent data. Final monoclinic cell parameters and their estimated standard deviations were obtained from the same crystal by a least-squares fit to 2θ values of 12 reflections randomly distributed in reciprocal space ($27° < 2\theta < 44°$) which were tuned for both Friedel-related peaks; the result was a = 6.821(2), b = 3.741(1), c = 14.937(3) Å, and β = 95.66(3)°. The edges of the crystals lie parallel to the cell axes and the crystal dimensions are inversely related to the axial lengths.

Structure Determination

The unit cell was indicated to be centric, based on a Howells–Phillips–Rodgers test of the intensity distribution, and since no extinction conditions were noted the monoclinic space group $P2/m$ was chosen. Placement of all atoms on the mirror planes at y = 0.0 or 0.5 appeared likely based on the short b axis, 3.74 Å, which is essentially the van der Waals diameter of iodine.

Trial atom positions were obtained by a direct method using MULTAN (*13*). Several sets so produced were eliminated on the basis of chemical and structural common sense. After full-matrix least-square refinement of positional and isotropic thermal parameters for the best set, an $R = \Sigma||F_o|-|F_c||/\Sigma|F_o| = 0.107$ was obtained. Closer inspection of the structure and data set at this point revealed the existence of a two-fold screw axis ($0k0$, $k \neq 2n$ absent); therefore the correct space group is $P2_1/m$

TABLE I

CRYSTALLOGRAPHIC DATA AND ATOMIC PARAMETERS[a] FOR α-ZrI_2

Composition: ZrI_2
Cell: monoclinic, $P2_1/m$ (No. 11), Z = 4
Lattice parameters: a = 6.821(2) Å, b = 3.741(1) Å, c = 14.937(3) Å, β = 95.66(3)
Refinement: R = 0.064, R_w = 0.079 (669 reflections, $2\theta \leq 50°$)

	x	z	B_{11}[b]	B_{22}	B_{33}	B_{13}
I1	0.6031(3)	0.6095(1)	1.13(6)	0.53(6)	1.42(7)	0.07(2)
I2	0.4498(3)	0.1473(1)	1.47(7)	0.62(6)	1.18(7)	0.02(2)
I3	0.8881(3)	0.3528(1)	1.34(7)	0.57(6)	1.30(7)	−0.05(2)
I4	0.0545(3)	0.8901(1)	1.17(7)	0.58(7)	1.39(7)	−0.02(2)
Zr1	0.1892(4)	0.5036(2)	0.93(9)	0.76(8)	1.44(9)	−0.00(3)
Zr2	0.6880(4)	0.9969(2)	0.95(9)	0.81(8)	1.26(7)	−0.01(3)

[a] y = 0.25

[b] $T = \exp[(-\frac{1}{4}(B_{11}h^2a^{*2} + B_{22}k^2b^{*2} + B_{33}l^2c^{*2} + 2B_{12}hka^*b^* + 2B_{13}hla^*c^* + 2B_{23}klb^*c^*)]$; $B_{12} = B_{23} = 0$ by symmetry.

(No. 11) with all atoms on the special position 2*e*. Refinement with anisotropic thermal parameters then produced an $R = 0.071$ and an $R_w = 0.100$, where $R_w = [\Sigma w(|F_o|-|F_c|)^2/\Sigma w|F_o|^2]^{1/2}$ and $w = \sigma_F^{-2}$. Need for an absorption correction was indicated by elongation of the thermal ellipsoids along *b*, the shortest crystal axis. The correction utilized the program TALABS (*14*) and an absorption coefficient of $\mu = 190\ cm^{-1}$ (*15*), and the crystal was approximated as a rectangular box of extreme dimensions stated earlier. Because of the large differences in crystal dimensions, transmission coefficients varied from 0.25 to 0.82 and χ and φ settings for the faces were found to be critical. After this was completed ($R = 0.065$, $R_w = 0.115$) the stronger reflections were observed to have larger values of $w||F_o|-|F_c||$. The data were therefore reweighted in groups sorted on F_o to give final converged residuals $R = 0.064$ and $R_w = 0.079$, with a final shift/error of <0.001 for all atoms. The thermal ellipsoids were now more reasonably shaped, and the standard deviations were ~15% lower than before. A final Fourier difference synthesis map was flat to $\leq 1\ e/Å^3$ at all points.

Description of the Structure

Final positional and thermal parameters for the structure of α-ZrI_2 are listed in Table I and significant distances and angles, in Table II. Structure factor results are given in a supplementary table.[1]

[1] See NAPS document No. 03772 for 3 pages of supplementary material. Order from ASIS/NAPS c/o Microfiche Publications, P.O. Box 3513, Grand Central station, New York, New York 10017. Remit in advance for each NAPS Accession number. Institutions and organizations may use purchase orders when ordering; however, there is a billing charge for this service. Make checks payable to Microfiche Publications. Photocopies are $5.00. Microfiche are $3.00. Outside the U.S. and Canada, postage is $3.00 for a photocopy or $1.50 for a fiche.

An approximately [010] projection of the structure is shown in Fig. 1. The iodine positions can be related to h.c.p. layers normal to *c*, with metal atoms (solid) occupying all octahedral sites between alternate layers to form slabs analogous to those in the CdI_2 structure. In the present case, however, the metal atoms are displaced 0.440 Å from the centers of the octahedral sites toward shared edges of the polyhedra to form zigzag chains parallel to *b*. This displacement of the metal atoms causes the iodine layers in each slab to buckle, and packing of these buckled layers in effect requires a second slab with independent atoms. Equivalent distances in the two independent slabs all differ by less than 3σ (Table II) except that the $I4^e$–$I2^b$ and $I4^a$–I2 distances differ by 6σ (0.016 Å) in opposite directions.

The [001] projection in Fig. 2 shows two iodine layers and the intervening metal layer which lies at $z \approx 0$. The two iodine octahedra outlined share a common edge ($I2^b$ and I2) through which the presumed Zr–Zr bond passes. Edges of these polyhedra range between 3.74 and 4.47 Å except for the shared edge $I2^b$–I2 which is 4.89 Å. This elongation results when the adjacent shared edges of the occupied iodide octahedra are pushed apart to make room for the Zr–Zr bonds. Corresponding effects are observed in the zirconium–iodine distances.

The metal–metal distances in α-ZrI_2 are closely comparable to those in the cluster Zr_6I_{12} (β-ZrI_2) despite the lower number of metal neighbors in the former. The two Zr–Zr bonds per d^2 metals in α-ZrI_2 are formally single bonds but a substantial bonding restriction (matrix effect) is superimposed by the edge sharing of the distorted iodine octahedra, and the 3.182(2) Å distance observed corresponds to a Pauling bond order of only 0.31. In β-ZrI_2 each zirconium has pairs of metal neighbors in the Zr_6 octahedron at 3.195(1) Å and 3.204(2) Å. These are now formally bonded

TABLE II

IMPORTANT DISTANCES (Å) AND ANGLES (deg) IN THE TWO INDEPENDENT UNITS

Distances			
Zr–Zr, Intrachain			
2^f–2^a	3.183(3)	1–1^g	3.181(3)
2^a–2^c	3.741(1)	1^g–1^j	3.741(1)
Zr–Zr, Interchain			
2^f–2^i	4.642(4)	1–1^a	4.644(4)
Zr–I			
2^f–4^e	3.096(2)	1–1	3.099(3)
2^f–2	2.896(3)	1–3^h	2.895(3)
2^f–4^a	2.973(2)	1–1^a	2.973(2)
2^f–2^b	2.936(2)	1–3^a	2.933(2)
I–I, Intrasheet			
4^e–2^b	3.909(2)	1–3^a	3.925(2)
4^a–2	3.950(2)	1^a–3^h	3.934(2)
4^a–4^c	3.741(1)	1^a–1^c	3.741(1)
2^b–2^d	3.741(1)	3^a–3^c	3.741(1)
4^c–4^a	3.911(3)	1–1^a	3.914(3)
4^a–2^b	4.469(3)	1^a–3^a	4.470(2)
2^b–2	4.887(3)	3^a–3^h	4.884(3)
2–4^e	5.904(3)	3^h–1	5.902(3)
I–I, Intersheet			
1^a–2	4.132(2)		
4^a–3	4.136(2)		
4^a–1^a	5.885(3)		
3–2	4.068(2)		
2–3^h	5.143(2)		
1^a–4^g	4.948(3)		
Angles			
I–Zr–I, Coordination Polyhedra			
4^a–2^f–4^c	77.97(7)	1^a–1–1^c	77.97(6)
4^a–2^f–2^b	98.26(4)	1^a–1–3^a	98.35(4)
2^b–2^f–2^d	79.15(7)	3^a–1–3^c	79.23(6)
2^b–2^f–2^e	80.74(6)	3^a–1–1	81.13(6)
4^a–2^f–4^e	80.23(5)	1^a–1–1	80.23(6)
2^b–2^f–2	113.85(6)	3^a–1–3^h	113.84(6)
4^a–2^f–2	84.58(6)	1^a–1–3^h	84.18(6)
I–I–I, Intrasheet			
2^d–4^e–2^b	57.18(3)	3^c–1–3^a	56.92(3)
4^e–2^b–2^d	61.41(2)	1–3^a–3^c	61.54(2)
4^c–2–4^a	56.54(3)	1^c–3^h–1^a	56.78(3)
2–4^a–4^c	61.73(2)	3^h–1^a–1^c	61.61(2)

[a] $1-x, 1-y, 1-z$.
[b] $1-x, 1-y, \bar{z}$.
[c] $1-x, \bar{y}, 1-z$.
[d] $1-x, \bar{y}, \bar{z}$.
[e] $1+x, y, z-1$.
[f] $x, y, z-1$.
[g] $\bar{x}, 1-y, 1-z$.
[h] $x-1, y, z$.
[i] $2-x, 1-y, 1-z$.
[j] $\bar{x}, \bar{y}, 1-z$.

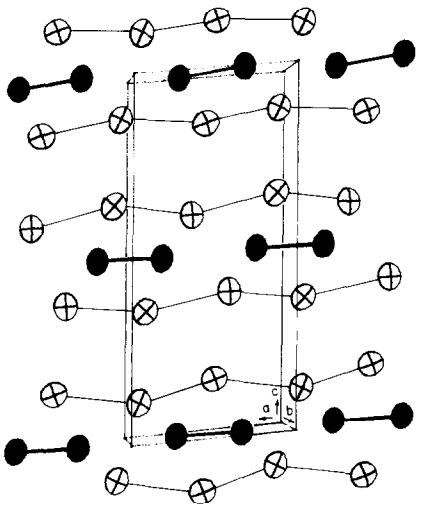

FIG. 1. The α-ZrI_2 structure viewed parallel to the zigzag metal chains and the short b axis. Zirconium and iodine atoms are represented by solid and open ellipsoids, respectively.

by half bonds and although repulsions between iodine atoms which bridge edges of the metal octahedron clearly restrict the approach of the metal atoms, this is not as severe as in α-ZrI_2. Since the metal-bonding electrons do not screen the iodine

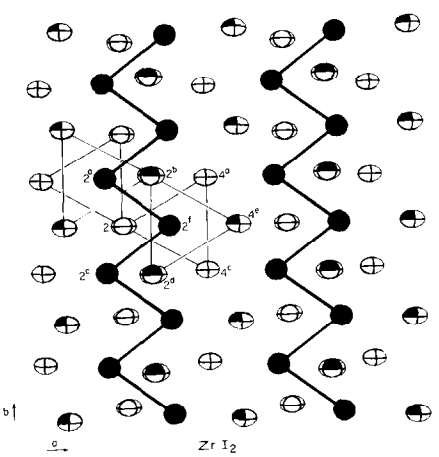

FIG. 2. View of two iodine layers and the intervening zigzag metal chains with two iodine octahedra which share a common edge outlined. All atoms lie on mirror planes at $y = 0.25$ and 0.75. The iodine atoms, partially darkened, lie toward the viewer.

atoms, the Zr–I distances are very similar throughout, 2.895(3)–2.973(2) Å for the closer five in α-ZrI_2 vs 2.860(2)–2.947(2) Å for the closer four in β-ZrI_2, and 2.863 Å for the average in ZrI_4 (*16*). The transformation from α- to β-ZrI_2 at high temperatures involves a loss of two Zr–I bonds and a gain of two Zr–Zr bonds, and is thought to be largely entropically driven to the more open structure (the center of the Zr_6 cluster corresponds to a missing iodine atom in a close-packed layer).

The metal–metal interactions in the α-ZrI_2 chains still must be classed as "strong" since the 3.182 Å separation is less than the 3.204 Å average distance found in the (12-coordinate) metal. The result is a filled-band semiconductor experimentally, with $\rho = 22$ ohm-cm and $E_g \simeq 0.1$ eV at room temperature according to four-probe measurements. No esr signal is observed at 94.7 Hz at either 20 or −196°C. In a localized sense one can view the σ bonds as generated by d_{xz} and $d_{z^2-y^2}$ orbitals, and these generate a filled band.

Discussion

The α-ZrI_2 described here is isostructural and isoelectronic with β-$MoTe_2$ (*17*), and as such represents the first halide found with this particular structure. A considerable similarity also exists with the higher-symmetry WTe_2 (space group $Pnm2_1$), the only difference being a smaller displacement of one slab with respect to another so that the β-angle (Fig. 1) decreases to 90° and an n glide develops parallel to c. In fact an incipient n glide in that direction is evident in the positional parameters in α-ZrI_2 except for x coordinates of the iodine atoms (Table I). In contrast with α-ZrI_2 however, $MoTe_2$ is a semimetal with $\rho = 2 \times 10^{-3}$ ohm-cm at 25°C (*18*).

Structural similarities between reduced metal sulfides and selenides with those involving isoelectronic chloride and bromide

anions are relatively rare. A direct relationship exists between MoS_2 and one polymorph of $ZrCl_2$ (*4*) as both have the $3R$-MoS_2-type layered structure with trigonal prismatic coordination of the metals, while a lesser element of similarity occurs between Hf_2S (*19*) and HfCl (*8*), where both contain infinite double metal layers but these are separated by different number of nonmetal layers. The lack of more S vs Cl and Se vs Br structural similarities has been attributed to the greater covalency of the chalcide relative to that in the isoelectronic halide (*20*). Not surprisingly, iodine, which bonds more covalently, exhibits a larger number of isostructural relationships with the chalcides. Examples of these include PrI_2 and MoS_2 ($2H_1$ and $3R$ types), GdI_2 and MoS_2 ($2H_1$) (*21*), ThI_2 and 4H–NbS_2 (*22*), and that seen here for β-$MoTe_2$ and α-ZrI_2. Even so, mixing of iodide and metal valence orbitals is presumably less, making the bands narrower and metallic conduction less prevalent than in the chalcides.

An indication of the M–M bond strength in α-ZrI_2 and similar distorted structures may be found in the magnitude of the lattice strain which accompanies M–M bond formation, specifically the amount of polyhedral distortion reflected in the ratio of the shortest to the longest M–X bonds (*18*). These ratios are 0.935, 0.959, and 0.962 for α-ZrI_2, β-$MoTe_2$, and WTe_2, respectively, indicating that α-ZrI_2 has the strongest M–M bonds or the weakest M–X bonds. On the other hand the metal–metal distances in both β-$MoTe_2$ and α-ZrI_2 are comparable, being 10.5 and 10.7% greater than the corresponding single-bond distances. Thus relative to the semimetallic β-$MoTe_2$ the stronger M–M bonding or greater distortion in α-ZrI_2 combined with the greater separation of atomic orbital energies for zirconium and iodine causes a separation of a filled valence band and the empty conduction band and gives a semiconducting α-ZrI_2.

The adoption of a distorted CdI_2 type for these compounds can easily be understood in terms of the extra stability obtained from the formation of two relatively short M–M bonds. The possibility of an α-$ZrI_2 \rightarrow \beta$-ZrI_2 transition at an observable rate seems remote, as this would require more than a simple intralayer rearrangement of the metal atoms, although such a transition is thought to occur by a topotactic path between the $CdCl_2$-type structure of PrI_2 (IV) and the cluster $(Pr_4I_4)I_4$ (type V) form (*21*). The transition from the α-ZrI_2 structure ($P2_1/m$) to an undistorted CdI_2-type ($P\bar{3}ml$) structure, which requires only an intralayer displacement of the metal atoms, is allowed by Landau's theory of second-order phase transitions (*23*) but is at present unknown. A similar transition has been observed between the MnP- and NiAs-type structures of VS (*24*). In addition there also exists the possibility of a low-temperature first-order phase transition in α-ZrI_2 to the $Pnm2_1$ structure of WTe_2. This has been observed for (metastable) β-$MoTe_2$, where the β angle varies discontinuously from 93.92° ($P2_1/m$) to 90° ($Pnm2_1$) within the temperature range $17 \rightarrow -40$°C (*25*), the low-temperature orthorhombic structure thus being produced via a shear deformation of the nonmetal layers perpendicular to the c axis. The pseudosymmetry relating atomic coordinates in the present structure (Table I) that was noted earlier reflects this potential.

A series of orthorhombic zirconium diiodides has recently been reported (*26*) which had cell parameters: $a = 3.74$ Å, $b = 6.93$ Å, $c = n \times 14.85$ Å, where the $n = 24$ polytype was studied the most. These were obtained in the temperature range 760–780°C and were thought to contain "alternating I–Zr–I double layers." Since the axial lengths are similar to those reported here, these may represent polytypes of a WTe_2-type structure or, less likely, 2H-

CdI_2, with pairs of three-layer slabs in the simple unit.

Acknowledgments

The authors thank Professor R. A. Jacobson and his group for assistance and the use of the diffractometer and computing systems, and Dr. T. Hsiang for the four-probe resistivity measurements.

References

1. J. D. CORBETT, R. L. DAAKE, K. R. POEPPELMEIER, AND D. H. GUTHRIE, *J. Amer. Chem. Soc.* **100,** 652 (1978).
2. H. IMOTO, J. D. CORBETT, AND A. CISAR, *Inorg. Chem.*, **20,** 145 (1981).
3. S. I. TROYANOV AND V. I. TSIREL'NIKOV, *Russ. J. Phys. Chem.* **48,** 1174 (1974). (Translation)
4. A. CISAR, J. D. CORBETT, AND R. L. DAAKE, *Inorg. Chem.* **18,** 836 (1979).
5. A. W. STRUSS AND J. D. CORBETT, *Inorg. Chem.* **9,** 1373 (1970).
6. S. I. TROYANOV, *Vestn. Mosk. Univ. Khim.* **28,** 369 (1973).
7. D. G. ADOLPHSON AND J. D. CORBETT, *Inorg. Chem.* **15,** 1820 (1976).
8. R. L. DRAKE AND J. D. CORBETT, *Inorg. Chem.* **16,** 2029 (1977).
9. R. L. DAAKE AND J. D. CORBETT, *Inorg. Chem.* **17,** 1192 (1978).
10. F. R. SALE AND R. A. SHELTON, *J. Less-Common Metals* **9,** 60 (1965).
11. K. R. POEPPELMEIER AND J. D. CORBETT, *J. Amer. Chem. Soc.* **100,** 5039 (1978).
12. W. L. ROHRBAUGH AND R. A. JACOBSON, *Inorg. Chem.* **13,** 2535 (1974).
13. P. MAIN, M. M. WOOLFSON, AND F. GERMAN, "MULTAN, a Computer Program for the Automatic Solution of Crystal Structures," Univ. of York Printing Unit, York (1971).
14. J. D. SCOTT, private communication (1971).
15. "International Tables for X-ray Crystallography," Vol. III, 2nd ed., Kynoch Press, Birmingham (1962).
16. B. KREBS, G. HENKEL, AND M. DARTMANN, *Acta Crystallogr. Sect. B* **35,** 274 (1979).
17. B. E. BROWN, *Acta Crystallogr.* **20,** 268 (1966).
18. J. A. WILSON AND A. D. YOFFE, *Adv. Phys.* **18,** 193 (1969).
19. H. F. FRANZEN AND J. GRAHAM, *Z. Kristallogr.* **123,** 133 (1966).
20. J. D. CORBETT, *Adv. Chem. Ser.* **186,** 329 (1980).
21. E. WARKENTIN AND H. BÄRNIGHAUSEN, *Z. Anorg. Allg. Chem.* **459,** 187 (1979).
22. L. J. GUGGENBERGER AND R. A. JACOBSON, *Inorg. Chem.* **7,** 2257 (1968).
23. L. D. LANDAU AND E. M. LIFSHITZ, "Statistical Physics," Chap. 14, Pergamon, London (1962).
24. H. F. FRANZEN, C. HAAS, AND F. JELLINEK, *Phys. Rev. B* **10,** 1248 (1974).
25. R. CLARKE, E. MARSEGLIA, AND H. P. HUGHES, *Philos. Mag.* **38,** 121 (1978).
26. KH. S. LOPIS, S. I. TROYANOV, AND V. I. TSIREL'NIKOV, *Russ. J. Inorg. Chem.* **24,** 1306 (1979). (Translation)